Journal of Engineering Mathematics (2005) 53: 1–20
DOI 10.1007/s10665-005-5571-6

Computation of Stokes flow due to the motion or presence of a particle in a tube

C. POZRIKIDIS
Department of Mechanical and Aerospace Engineering, University of California, San Diego, La Jolla, California 92093-0411, USA (cpozrikidis@ucsd.edu)

Received 23 April 2004; accepted in revised form 8 April 2005

Abstract. The computation of Stokes flow due to the motion or presence of a rigid particle in a fluid-filled tube with arbitrary geometry is discussed with emphasis on the induced upstream to downstream pressure change. It is proposed that expressing the pressure change as an integral over the particle surface involving (*a*) the *a priori* unknown traction, and (*b*) the velocity of the pure-fluid pressure-driven flow, simplifies the numerical implementation and ameliorates the effect of domain truncation. Numerical computations are performed based on the integral formulation in conjunction with a boundary-element method for a particle translating and rotating inside a cylindrical tube with a circular cross-section. The numerical results are consistent with previous asymptotic solutions for small particles, and complement available numerical solutions for particular types of motion.

Key words: boundary-element method, particles, Stokes flow, tube flow

1. Introduction

When a particle translates and rotates under the influence of gravity or another external force in a liquid-filled tube that is closed at both ends, it generates a pressure rise between the two ends. If the tube is open at the ends and exposed to the same ambient pressure, the particle motion causes a net longitudinal flow rate. The pressure rise established in the case of a closed tube is precisely equal to that necessary to annihilate the flow inside the open tube. A similar situation occurs in the case of a particle that is freely suspended in pressure-driven tube flow, depending on whether the axial flow rate or pressure difference due to the presence of the particle is required to be zero. Multi-particle arrangements in fluid-filled conduits and suspensions in tube flow behave in a similar fashion, with the particles making additive contributions to the pressure rise or flow rate. Interest in describing the hydrodynamics of these systems is motivated by applications in biomechanics, with particular interest in blood flow in the microcirculation, as well as by engineering applications involving particulate flow through porous media and the motion of small particles, macromolecules, and cells in fabricated microchannels.

A number of authors dating back to Happel and Byrne [1] have discussed the computation of the force, torque, and pressure change due to the motion or presence of a spherical particle, or a periodic file of spherical particles, in a cylindrical tube with a circular cross-section. Asymptotic results for small particles and numerical results for arbitrarily sized particles positioned along the tube axis in axisymmetric flow were presented by Happel and Byrne [1], Haberman and Sayre [2], and Wang and Skalak [3]. Asymptotic results for particles translating off the tube axis in non-axisymmetric flow were presented by Greenstein and Happel [4] and Tözeren [5,6], and numerical results based on finite-element and boundary-element

methods were presented by Tözeren [7], Graham *et al.* [8], Ingber [9] Mondy *et al.* [10], and Higdon and Muldowney [11]. The complementary problem of flow due to particle rotation was also addressed by several authors for axisymmetric and non-axisymmetric flow, as reviewed by Zheng *et al.* [12]. Unfortunately in only a few of these studies the pressure rise induced by the particle presence or motion was considered [1,3,4]. Instead, most authors have concentrated on the computation of the hydrodynamic force and torque exerted on a fixed or moving particle. In an extension of their earlier work motivated by applications in biomechanics, Chen and Skalak [13] considered axisymmetric flow past a file of oblate or prolate spheroidal particles oriented along the axis of a circular tube. Other authors derived asymptotic results for tightly fitting particles that nearly occlude the tube cross-section, as well as for small particles with arbitrary shape moving inside tubes with arbitrary cross-section, as reviewed by Falade and Brenner [14].

The present work is motivated by a desire to develop an efficient numerical method that is capable of handling particles with arbitrary shape and size, and tubes with arbitrary cross-section and possibly curved and tapered shapes. The point of departure is the boundary-integral formulation of Stokes flow, resulting in a Fredholm integral equation of the first kind for the boundary traction, which is solved by a boundary-element method. In this approach, the boundary of the computational domain, including the tube surface, the particle surface, and possibly the surface of two physical or artificial tube caps, are discretized into boundary elements, and the element traction is approximated with a polynomial expansion. One concern in the implementation of the numerical method is the choice of boundary conditions at the top and bottom tube caps. If the flow rate is specified, the method requires incorporating the *a priori* unknown upstream to downstream pressure difference due to the particle presence or motion, Δp, in the integral formulation. On the other hand, if Δp is specified, the method requires incorporating the *a priori* unknown streamwise flow rate. Because of the linearity of the equations of Stokes flow, one choice yields the other by rescaling. Specifying the flow rate instead of the pressure drop is more convenient in the numerical implementation.

Higdon and Muldowney [11] computed resistance functions for spherical particles in cylindrical tubes using a highly accurate spectral boundary-element method, and deduced Δp as part of the solution by imposing a constraint on the axial flow rate. The authors argued that using the traction boundary condition involving Δp instead of the velocity boundary condition at the tube caps minimizes the effect of domain truncation. However, in light of the uniqueness of Stokes flow, the stress boundary conditions should imply the velocity boundary condition, and *vice versa*, and the two choices should be identical. Ingber [9] and Mondy *et al.* [10] are silent on the issue of the top and bottom boundary conditions, and most likely perform the usual element discretization of all boundaries, and solve for the normal and tangential components of the traction.

In this article, it is shown that expressing the top to bottom pressure difference Δp as an integral over the particle surface involving the traction and the velocity of the undisturbed pure-fluid pressure-driven flow, yields an efficient numerical method that allows us to obtain reasonably accurate results even for crude particle and tube surface discretizations, and thereby ameliorates the effect of domain truncation. Though numerical results will be presented using an entry-level boundary-element method where the hydrodynamic traction is approximated with a constant function over the individual elements, extending the basic formulation to high order and spectral element methods is straightforward. An analogous integral representation for the induced pressure difference is also possible for flow past bubbles, drops, and capsules through tubes, as will be discussed in the concluding section.

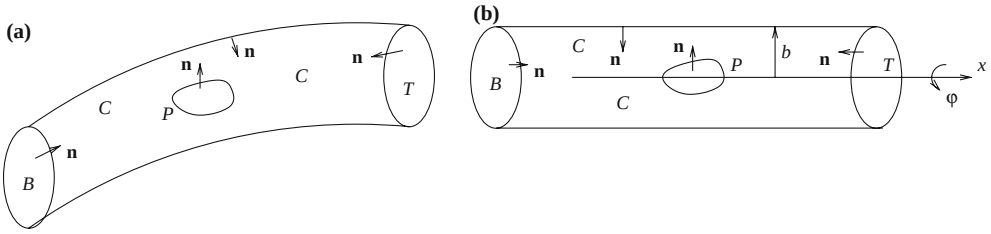

Figure 1. (a) Schematic illustration of Stokes flow in a tube due to the motion of, or past a rigid particle. (b) Flow in a cylindrical tube with a circular cross-section of radius b.

2. Problem statement and integral formulation

Consider a rigid particle translating and rotating inside a liquid-filled tube that is closed at both ends in an otherwise quiescent fluid, as shown in Figure 1(a). If the tube caps are sufficiently far from the particle, the fluid near the caps is virtually stationary, and the pressure assumes the value p_B over the bottom cap, and the value p_T over the top cap. The primary objective of the analysis is to evaluate the force and torque exerted on the particle, as well as the pressure rise $\Delta p \equiv p_T - p_B$, as a function of the particle shape and size relative to the tube.

If the flow occurs at sufficiently small Reynolds numbers, the velocity field induced by the particle motion, $\mathbf{u}$, can be described by the integral representation of Stokes flow as

$$u_j(\mathbf{x}_0) = -\frac{1}{8\pi\mu} \iint_{P,C,B,T} G_{ij}(\mathbf{x}, \mathbf{x}_0) f_i(\mathbf{x}) \mathrm{d}S(\mathbf{x}), \tag{2.1}$$

where μ is the fluid viscosity, $\mathbf{f} \equiv \boldsymbol{\sigma} \cdot \mathbf{n}$ is the surface traction, $\boldsymbol{\sigma}$ is the Newtonian stress tensor, $\mathbf{n}$ is the unit normal vector pointing into the fluid, and P, C, B, T stand, respectively, for the surface of the particle, the surface of the conduit represented by the tube, and the surface of the bottom and top tube caps, as shown in Figure 1(a) (*e.g.*, [15]). The kernel of the integral representation, G_{ij}, is the Stokes flow free-space Green's function, given by

$$G_{ij}(\mathbf{x}, \mathbf{x}_0) = \frac{\delta_{ij}}{|\mathbf{x} - \mathbf{x}_0|} + \frac{(x_i - x_{0_i})(x_j - x_{0_j})}{|\mathbf{x} - \mathbf{x}_0|^3}, \tag{2.2}$$

where δ_{ij} is Kronecker's delta. Physically, $G_{ij}(\mathbf{x}, \mathbf{x}_0)/(8\pi\mu)$ is the ith velocity component at the point $\mathbf{x}$ due to a point force of unit strength located at the point $\mathbf{x}_0$, pointing in the jth direction.

Theoretical analyses have shown that the velocity due to the particle motion decays exponentially with distance along the tube axis toward the profile of a pressure-driven flow (*e.g.*, [16]). If the induced flow rate is zero, as presently assumed, the velocity decays exponentially, and the pressure tends toward an upstream and a downstream value. Liron and Shahar [16] and Blake [17] showed that, in the case of an infinite circular cylinder of radius b, and when the particle is modeled as a point force positioned at the centerline pointing along the cylinder axis, decay occurs through an infinite sequence of toroidal eddies with approximate wave length $\lambda \simeq 2{\cdot}15b$. The rate of decay is approximately $\exp(-4{\cdot}47x/a)$, which means that it takes approximately one tube radius for the velocity to decay to 1% of the value multiplying the exponential. Given this fast decay, it is unlikely that corner eddies and other end-effects have any significant influence in the overall structure of the flow. In the case of a closed, semi-infinite or finite circular cylinder, decay occurs through a finite sequence of toroidal eddies that terminate at the caps [17]. It is then reasonable to write

$$\mathbf{f} \simeq -p_B \mathbf{n} + O(\exp(-Ad), \tag{2.3}$$

over the bottom cap, where A is a positive constant, and d is the distance of the particle from the bottom cap. Introducing the approximation, $\mathbf{f} \simeq -p_B \mathbf{n}$ over the bottom cap, and likewise, $\mathbf{f} \simeq -p_T \mathbf{n}$ over the top cap, reduces the integral representation (2.1) to

$$u_j(\mathbf{x}_0) = -\frac{1}{8\pi\mu}\Big[\iint_{P,C} G_{ij}(\mathbf{x}, \mathbf{x}_0) f_i(\mathbf{x}) \mathrm{d}S(\mathbf{x}) - p_B \iint_B G_{ij}(\mathbf{x}, \mathbf{x}_0) n_i(\mathbf{x}) \mathrm{d}S(\mathbf{x}) - p_T \iint_T G_{ij}(\mathbf{x}, \mathbf{x}_0) n_i(\mathbf{x}) \mathrm{d}S(\mathbf{x}) \Big]. \tag{2.4}$$

The force exerted on the particle, and the torque with respect to the designated particle center, $\mathbf{x}_c$, exerted on the particle are given by

$$\mathbf{F} = \iint_P \mathbf{f} \mathrm{d}S, \quad \mathbf{T} = \iint_P (\mathbf{x} - \mathbf{x}_c) \times \mathbf{f} \mathrm{d}S. \tag{2.5}$$

These integrals can be computed after the solution for the boundary traction, $\mathbf{f}$, and simultaneously for the pressures p_B and p_T have been found.

A standard method of computing the flow due to the particle motion involves discretizing the surface of the particle, P, and the surface of the conduit, C, into boundary elements, applying the integral representation at collocation points located at element centroids, and enforcing the no-slip and no-penetration boundary conditions to derive a system of linear equations for the boundary-element tractions. Since the pressure is only defined up to arbitrary constant, we may set without loss of generality $p_B = 0$. One more equation is required for computing the pressure over the top cap, p_T. In principle, this equation can arise by introducing a collocation point at the bottom or top cap. A serious drawback of this method is a pronounced numerical sensitivity, and the need to evaluate with high accuracy pertinent boundary integrals.

An alternative formulation employs the Green's function for Stokes flow in the tube under consideration, denoted by $\mathcal{G}_{ij}(\mathbf{x}, \mathbf{x}_0)$. Physically, $\mathcal{G}_{ij}(\mathbf{x}, \mathbf{x}_0)/(8\pi\mu)$ is the ith velocity component at the point $\mathbf{x}$ due to a point force of unit strength located at the point $\mathbf{x}_0$ pointing in the jth direction, subject to the conditions of zero velocity over the tube wall, and decaying velocity upstream and downstream, far from the point force. The boundary-integral formulation provides us with an integral representation for the velocity field as a single-layer potential over the particle surface alone,

$$u_j(\mathbf{x}_0) = -\frac{1}{8\pi\mu} \iint_P \mathcal{G}_{ij}(\mathbf{x}, \mathbf{x}_0) f_i(\mathbf{x}) \mathrm{d}S(\mathbf{x}), \tag{2.6}$$

thereby bypassing the computation of the induced pressure difference. Unfortunately, the Green's function for tube flow is available only for a cylindrical conduit with a circular cross-section due to Hirschfeld [18], Hasimoto [19], Liron and Shahar [16], Blake [17], and Hirschfeld *et al.* [20]. Even so, the evaluation of the final expressions carries a heavy computational burden because of the presence of a multitude of Bessel functions. For periodic flows and more general tube geometries, the Green's function can be computed by numerical methods and then reproduced from look-up tables, though the interpolation introduces further sources of numerical error [21].

2.1. Integral representation for the streamwise pressure difference

To compute the tube cap pressure difference, we apply the Lorentz reciprocal theorem of Stokes flow (*e.g.*, [15,22]) for a pair of flows consisting of (*a*) the flow due to the particle

motion presently considered, and (*b*) pressure-driven flow through the conduit in the absence of the particle, denoted by the superscript PDF, and obtain

$$\iint_{P,C,B,T} \mathbf{u}\cdot\mathbf{f}^{PDF}\,\mathrm{d}S = \iint_{P,C,B,T} \mathbf{u}^{PDF}\cdot\mathbf{f}\,\mathrm{d}S. \tag{2.7}$$

Since the velocity of both flows is zero over the conduit surface, $\mathbf{u}=\mathbf{0}$ and $\mathbf{u}^{PDF}=\mathbf{0}$ on C, and the velocity due to the particle motion is almost zero over the bottom and top caps of a long tube, $\mathbf{u}\simeq\mathbf{0}$ on B, T, the corresponding integrals in (2.7) disappear. Introducing the aforementioned approximation $\mathbf{f}\simeq -p_B\mathbf{n}$ over the bottom cap and $\mathbf{f}\simeq -p_T\mathbf{n}$ over the top cap, and simplifying, we find

$$\iint_{P} \mathbf{u}\cdot\mathbf{f}^{PDF}\,\mathrm{d}S = \iint_{P} \mathbf{u}^{PDF}\cdot\mathbf{f}\,\mathrm{d}S - (p_B - p_T)Q^{PDF}, \tag{2.8}$$

where

$$Q^{PDF} \equiv \iint_{B} \mathbf{u}^{PDF}\cdot\mathbf{n}\,\mathrm{d}S = -\iint_{T} \mathbf{u}^{PDF}\cdot\mathbf{n}\,\mathrm{d}S \tag{2.9}$$

is the streamwise flow rate of the pressure-driven flow in the absence of the particle. Setting the velocity over the particle surface equal to $\mathbf{u}=\mathbf{V}+\boldsymbol{\Omega}\times(\mathbf{x}-\mathbf{x}_c)$, where $\mathbf{V}$ is the translational velocity of the designated particle center, $\mathbf{x}_c$, and $\boldsymbol{\Omega}$ is the particle angular velocity about $\mathbf{x}_c$, we find

$$\mathbf{U}\cdot\iint_{P} \mathbf{f}^{PDF}\,\mathrm{d}S - \boldsymbol{\Omega}\cdot\iint_{P} (\mathbf{x}-\mathbf{x}_c)\times\mathbf{f}^{PDF}\,\mathrm{d}S = \iint_{P} \mathbf{u}^{PDF}\cdot\mathbf{f}\,\mathrm{d}S - (P_B - P_T)Q^{PDF}. \tag{2.10}$$

Force and torque equilibrium in Stokes flow require that the two integrals on the left-hand side are zero. Rearranging the resulting equation, we obtain Brenner's [23] integral representation

$$\Delta p \equiv p_T - p_B = -\frac{1}{Q^{PDF}}\iint_{P} \mathbf{u}^{PDF}\cdot\mathbf{f}\,\mathrm{d}S, \tag{2.11}$$

which provides us with an expression for the pressure difference, Δp, in terms of the *a priori* unknown traction over the particle surface and the velocity of the unperturbed pressure-driven flow, to be used instead of point collocation over the top or bottom tube cap. It is reassuring to observe that the traction over the particle surface inside the integral on the right-hand side of (2.11) can be enhanced with an arbitrary multiple of the normal vector. Because the velocity field of the pressure-driven flow is assumed to be solenoidal, $\iint_P \mathbf{u}^{PDF}\cdot\mathbf{n}\,\mathrm{d}S=0$, this modification does not alter the computed pressure change.

Physically, the integral representation (2.11) expresses the additive contribution of the pressure differences due to point forces distributed over the particle surface, where the strength of the point forces is equal to the negative of the particle surface traction. In fact, comparing (2.11) with (2.6), we find that the pressure difference associated with the tube-flow Green's function is given by

$$\Delta\mathcal{P}_i(\mathbf{x}_0) = \frac{8\pi}{Q^{PDF}}u_i^{PDF}(\mathbf{x}_0). \tag{2.12}$$

This formula can be derived independently, by applying once again the Lorentz reciprocal theorem for the pressure-driven flow and the singular flow induced by a point force in the

absence any particles, with velocity $\mathbf{u}$ and stress $\boldsymbol{\sigma}$. Simplifying by use of the boundary conditions, we find

$$\iint_{B,T} \mathbf{u}^{PDF} \cdot \mathbf{f}\, \mathrm{d}S = -\iiint \mathbf{u}^{PDF} \cdot \nabla \cdot \boldsymbol{\sigma}\, \mathrm{d}V, \tag{2.13}$$

where the volume integral on the right-hand side is computed over the volume of the tube enclosed by the tube wall and end caps. To complete the proof, we write

$$\Delta p = \frac{1}{8\pi} \Delta \mathcal{P}_i b_i, \quad \nabla \cdot \boldsymbol{\sigma} = -\delta(\mathbf{x} - \mathbf{x}_0)\mathbf{b}, \tag{2.14}$$

where $\mathbf{b}$ is the vectorial strength of the point force, and δ is Dirac's three-dimensional delta function. Substituting these expressions in (2.13) and simplifying, we obtain (2.12).

2.2. Small-particle asymptotics

When the particle size is small compared to the linear dimension of the tube cross-section, we may evaluate the velocity of the pressure-driven flow inside the integral on the right-hand side of (2.11) at a designated particle center, $\mathbf{x}_c$, to obtain Brenner's approximation [23]

$$\Delta p \simeq -\frac{1}{Q^{PDF}} \mathbf{u}^{PDF}(\mathbf{x}_c) \cdot \mathbf{F}. \tag{2.15}$$

At this level, we may also approximate the actual force exerted on the particle, $\mathbf{F}$, with the force exerted on the particle when it moves in an infinite fluid, $\mathbf{F}^{\infty}$. The linearity of the equations of Stokes allows us to write

$$\mathbf{F}^{\infty} \equiv -\mu \mathbf{R}^{\infty} \cdot \mathbf{Q}, \tag{2.16}$$

where $\mathbf{Q} = [V_x, V_y, V_z, \Omega_x, \Omega_y, \Omega_z]^T$ is the generalized particle velocity vector, and $\mathbf{R}^{\infty}$ is the 6×6 grand resistance tensor for flow in an infinite fluid. For example, in the case of a spherical particle of radius a whose centered is placed at the point $\mathbf{x}_c$ inside the tube, we use Stokes' law and invoke the reversibility of Stokes flow to find $\mathbf{R}^{\infty} = 6\pi\mu a[\mathbf{I}, \mathbf{0}]$, where $\mathbf{I}$ is the 3×3 unit matrix and $\mathbf{0}$ is the 3×3 null matrix. Substituting (2.16) in (2.15), we derive the asymptotic expression

$$\Delta p \simeq \frac{\mu}{Q^{PDF}} \mathbf{u}^{PDF}(\mathbf{x}_c) \cdot \mathbf{R}^{\infty} \cdot \mathbf{Q}. \tag{2.17}$$

2.3. Numerical implementation

To illustrate the implementation of the numerical method based on the formulation described previously in this section, we set $p_B = 0$, and recast the integral representation (2.4) into the form

$$\iint_{P,C} G_{ij}(\mathbf{x}, \mathbf{x}_0) f_i(\mathbf{x}) \mathrm{d}S(\mathbf{x}) - p_T \iint_T G_{ij}(\mathbf{x}, \mathbf{x}_0) n_i(\mathbf{x}) \mathrm{d}S(\mathbf{x}) = -8\pi\mu u_j(\mathbf{x}_0). \tag{2.18}$$

Next, we discretize the tube (conduit) surface into N_C boundary elements and the particle surface into N_P boundary elements, and approximate the components of the traction with constant functions over each element. The no-slip and no-penetration boundary conditions require that $\mathbf{u} = \mathbf{0}$ over the conduit elements, and $\mathbf{u} = \mathbf{V} + \boldsymbol{\Omega} \times (\mathbf{x} - \mathbf{x}_c)$ over the particle elements. Identifying the evaluation point $\mathbf{x}_0$ in (2.18) sequentially with the particle and cylinder

element centroids, and appending to the resulting system of algebraic equations the discretized version of the integral representation (2.11) with $p_B = 0$, we derive the master linear system

$$\left[\begin{array}{c|c|c} \mathbf{P}_P & \mathbf{P}_C & \mathbf{p}_T \\ \hline \mathbf{C}_P & \mathbf{C}_C & \mathbf{c}_T \\ \hline \mathbf{w}_P & \mathbf{0} & 1 \end{array}\right] \cdot \left[\begin{array}{c} \mathbf{f}_P \\ \mathbf{f}_C \\ p_T \end{array}\right] = \left[\begin{array}{c} \mathbf{b}_P \\ \mathbf{0} \\ 0 \end{array}\right], \tag{2.19}$$

subject to the following definitions:

- $\mathbf{P}_P$ is a $3N_P \times 3N_P$ particle self-influence matrix, $\mathbf{P}_C$ is a $3N_P \times 3N_C$ particle-cylinder influence matrix, $\mathbf{C}_P$ is a $3N_C \times 3N_P$ cylinder-particle influence matrix, and $\mathbf{C}_C$ is a $3N_C \times 3N_C$ cylinder self-influence matrix, The influence matrices are defined in terms of the single-layer potential over the boundary elements.
- The $3N_P$-dimensional horizontal vector $\mathbf{w}_P$ is defined such that

  $$\mathbf{w}_P \cdot \mathbf{f}_P + p_T = 0 \tag{2.20}$$

  is the discrete representation of (2.11) with $p_B = 0$. The adjacent entry, $\mathbf{0}$, is a $3N_C$-dimensional horizontal null vector.
- The $3N_P$-dimensional vertical vector $\mathbf{p}_T$ and corresponding $3N_C$-dimensional vertical vector $\mathbf{c}_T$ contain the xx, xy, and xz components of the single-layer potential integrated over the top cylinder cap and evaluated, respectively, at the particle and cylinder collocation points.
- The vector of unknowns on the left-hand side of (2.19) is comprised of a $3N_P$-dimensional vector holding the Cartesian components of the particle-element tractions, $\mathbf{f}_P$, a $3N_C$-dimensional vector holding the Cartesian components of the cylinder-element tractions, $\mathbf{f}_C$, and the scalar top-cap pressure, p_T.
- The vector $\mathbf{b}_P$ on the right-hand side of (2.19) encapsulates the right-hand side of the integral equation (2.18) evaluated at the particle collocation points.

A test of accuracy in the evaluation of the influence matrices can be performed based on the integral identities

$$\iint_P G_{ij}(\mathbf{x}, \mathbf{x}_0) n_i(\mathbf{x}) \mathrm{d}S(\mathbf{x}) = 0, \quad \iint_{C,B,T} G_{ij}(\mathbf{x}, \mathbf{x}_0) n_i(\mathbf{x}) \mathrm{d}S(\mathbf{x}) = 0, \tag{2.21}$$

for an arbitrary evaluation point, $\mathbf{x}_0$, originating from the continuity equation (*e.g.*, [15]). The discretized versions of these identities are

$$\begin{aligned} &\mathbf{P}_P \cdot \mathbf{n}_P = \mathbf{0}, \\ &\mathbf{C}_P \cdot \mathbf{n}_P = \mathbf{0}, \\ &\mathbf{P}_C \cdot \mathbf{n}_C + \mathbf{p}_B \cdot \mathbf{n}_B + \mathbf{p}_T \cdot \mathbf{n}_T = \mathbf{0}, \\ &\mathbf{C}_C \cdot \mathbf{n}_C + \mathbf{c}_B \cdot \mathbf{n}_B + \mathbf{c}_T \cdot \mathbf{n}_T = \mathbf{0}, \end{aligned} \tag{2.22}$$

where the bottom-cap vectors, $\mathbf{p}_B$ and $\mathbf{c}_B$, are defined by analogy with the aforementioned top-cap vectors, $\mathbf{p}_T$ and $\mathbf{c}_T$, and the vector $\mathbf{n}_P$ holds the unit normal vector at the particle collocation points. The vectors $\mathbf{n}_C$, $\mathbf{n}_B$, and $\mathbf{n}_T$ are similarly defined. In the computations for a cylindrical tube with a circular cross-section of radius b discussed in Section 4, the right-hand sides of Equations (2.22) were confirmed to be on the order of $10^{-4}\ b$.

Once the master linear system (2.19) has been compiled, the solution can be found by block Jacobi diagonalization, based on the splitting

$$\left[\begin{array}{c|c|c} \mathbf{P}_P & \mathbf{0} & \mathbf{0} \\ \hline \mathbf{0} & \mathbf{C}_C & \mathbf{0} \\ \hline \mathbf{0} & \mathbf{0} & 1 \end{array}\right] \cdot \left[\begin{array}{c} \mathbf{f}_P \\ \mathbf{f}_C \\ p_T \end{array}\right] = \left[\begin{array}{c} \mathbf{b}_P \\ \mathbf{0} \\ 0 \end{array}\right] - \left[\begin{array}{c|c|c} \mathbf{0} & \mathbf{P}_C & \mathbf{p}_T \\ \hline \mathbf{C}_P & \mathbf{0} & \mathbf{c}_T \\ \hline \mathbf{w}_P & \mathbf{0} & 0 \end{array}\right] \cdot \left[\begin{array}{c} \mathbf{f}_P \\ \mathbf{f}_C \\ p_T \end{array}\right]. \tag{2.23}$$

The numerical procedure involves the following steps:

1. Assume $p_T = 0$ and $\mathbf{f}_C = \mathbf{0}$, which amounts to ignoring the presence of the tube.
2. Solve for the particle traction vector, $\mathbf{f}_P$, using the first block of (2.23).
3. Compute the top-cap pressure, p_T, using the third block of (2.23).
4. Compute the cylinder surface traction vector, $\mathbf{f}_C$, using the second block of (2.23).
5. Return to step 2 and repeat until convergence.

In the computations presented in Section 3 for a circular tube, the number of iterations for the error in the solution of the master linear system to become comparable to the discretization error ranges from 3 to 10, depending on the particle size relative to the tube radius. In the numerical implementation, the block-Jacobi iterations were carried out based on the inverses of the tube and particle self-interaction matrices, according to the symbolic algorithm

$$\left[\begin{array}{c} \mathbf{f}_P \\ \mathbf{f}_C \\ p_T \end{array}\right]^{(k+1)} = \left[\begin{array}{c|c|c} \mathbf{P}_P^{-1} & \mathbf{0} & \mathbf{0} \\ \hline \mathbf{0} & \mathbf{C}_C^{-1} & \mathbf{0} \\ \hline \mathbf{0} & \mathbf{0} & 1 \end{array}\right] \cdot \left(\left[\begin{array}{c} \mathbf{b}_P \\ \mathbf{0} \\ 0 \end{array}\right] - \left[\begin{array}{c|c|c} \mathbf{0} & \mathbf{P}_C & \mathbf{p}_T \\ \hline \mathbf{C}_P & \mathbf{0} & \mathbf{c}_T \\ \hline \mathbf{w}_P & \mathbf{0} & 0 \end{array}\right] \cdot \left[\begin{array}{c} \mathbf{f}_P \\ \mathbf{f}_C \\ p_T \end{array}\right]^{(k)} \right), \tag{2.24}$$

where the superscript (k) denotes the kth iteration.

Because the block-diagonal matrices and their inverses on the right-hand sides of (2.23) and (2.24) are independent of the *relative* location of the particle and cylinder, they need to be evaluated only once in studies of multiple configurations. Additional reduction in computational cost is possible on the observation that, if the particle is expanded or reduced by an arbitrary factor, the corresponding self-interaction matrix and its inverse are merely multiplied or divided by the expansion or shrinkage factor. Moreover, if the particle is rotated about an arbitrary direction, the new self-interaction matrix can be constructed using the standard rules of tensor transformation. Accordingly, these matrices need to be evaluated only for one particle size and orientation, and may then be rescaled or transformed to accommodate other particle sizes and orientations. Similar transformations are possible for the cylinder self-interaction matrix.

Now, because of the first integral identity in (2.21), the self-interaction matrix, $\mathbf{P}_P$, and the mutual-influence matrix, $\mathbf{C}_P$, are nearly singular. Consequently, the inverse matrix $\mathbf{P}_P^{-1}$ employed in the iterations is poorly conditioned. To overcome this difficulty, the integral equation is regularized by adding to the right-hand side of (2.1) the deflating term

$$n_i(\mathbf{x}_0) \iint_P \mathbf{n}(\mathbf{x}) \cdot \mathbf{f}(\mathbf{x}) \mathrm{d}S(\mathbf{x}), \tag{2.25}$$

which removes the null eigenvalue of the single-layer potential (*e.g.*, [15]).

Integrating the equations of Stokes flow over the volume of fluid enclosed by the tube and particle, we derive the global force balance

$$\mathcal{R} \equiv \iint_{P,C,B,T} \mathbf{f}\, \mathrm{d}S(\mathbf{x}) = \mathbf{0}, \tag{2.26}$$

where $\mathcal{R}$ stands for the residual. The satisfaction of (2.26) provides us with a measure of accuracy of the numerical method. In computations for a cylindrical tube with a circular cross-section of radius b, discussed in Section 4, the discrete representation of (2.26) is

$$\mathcal{R} \equiv \mathbf{A}_P \cdot \mathbf{f}_P + \mathbf{A}_C \cdot \mathbf{f}_C + \Delta P \pi b^2 \begin{bmatrix} 1 \\ 0 \\ 0 \end{bmatrix} = \begin{bmatrix} 0 \\ 0 \\ 0 \end{bmatrix}, \tag{2.27}$$

where the 3 rows of the $3 \times 3N_P$ matrix $\mathbf{A}_P$ contain the twice duplicated string of particle-element surface areas, and the 3 rows of the $3 \times 3N_C$ matrix $\mathbf{A}_C$ contain the twice duplicated string of cylinder-element surface areas. In the computations discussed in Section 3, the magnitude of the residual is less than 1% of the maximum term in (2.27).

3. Generalization to pressure-driven and periodic flow

In Section 2, we discussed the problem of particle motion in a closed or otherwise long tube, in an otherwise quiescent fluid. The derivations can be generalized to more general circumstances, including flow past a stationary or freely suspended particle, flow past a periodic arrangement of particles in a cylindrical tube with arbitrary cross-section, and flow past a multitude of particles in a suspension.

3.1. Particle motion in pressure-driven flow

Introducing a stationary or freely moving particle in a pressure-driven tube flow affects either the pressure change, or the flow rate, or both. For example, in pumping a suspension through a tube, we can either hold the flow rate constant, or the pumping head fixed, or vary both at will. A corresponding degree of freedom arises in the mathematical analysis of pressure-driven particulate flow. However, because of the linearity of the equations of Stokes flow, the results for one chosen set of conditions can be rescaled to describe any other condition.

Assuming that the perturbation velocity due to the particle decays far from the particle, and therefore the presence of the particle does not affect the streamwise flow rate, Q^{PDF}, we find that the perturbation velocity, $\mathbf{u}'$, is given by the counterpart of (2.4),

$$\begin{aligned} u'_j(\mathbf{x}_0) = -\frac{1}{8\pi\mu}\Big[& \iint_{P,C} G_{ij}(\mathbf{x}, \mathbf{x}_0) f_i(\mathbf{x}) \mathrm{d}S(\mathbf{x}) \\ & - p'_B \iint_B G_{ij}(\mathbf{x}, \mathbf{x}_0) n_i(\mathbf{x}) \mathrm{d}S(\mathbf{x}) - p'_T \iint_T G_{ij}(\mathbf{x}, \mathbf{x}_0) n_i(\mathbf{x}) \mathrm{d}S(\mathbf{x}) \Big], \end{aligned} \tag{3.1}$$

where a prime denotes a perturbation quantity. The additional pressure difference due to the particle is given by the counterpart of (2.11),

$$\Delta p' \equiv p'_T - p'_B = -\frac{1}{Q^{PDF}} \iint_P \mathbf{u}^{PDF} \cdot \mathbf{f}\, \mathrm{d}S. \tag{3.2}$$

The no-slip and no-penetration boundary conditions require that the velocity over the particle surface expresses rigid-body motion, $\mathbf{u} = \mathbf{u}^{PDF} + \mathbf{u}' = \mathbf{V} + \boldsymbol{\Omega} \times (\mathbf{x} - \mathbf{x}_c)$ or $\mathbf{u}' = -\mathbf{u}^{PDF} + \mathbf{V} + \boldsymbol{\Omega} \times (\mathbf{x} - \mathbf{x}_c)$

over the particle elements. In the boundary-element formulation, this boundary condition is implemented in the first vector block, $\mathbf{b}_P$, on the right-hand side of the linear system (2.19).

Alternatively, the force exerted on a particle that is held stationary in pressure-driven flow, $\mathbf{F}$, can be computed from the results of particle motion in a closed tube, without repeating the boundary-element solution. Applying the reciprocal theorem for this flow and the flow due to the particle translating with velocity $\mathbf{U}$ inside the tube in an otherwise quiescent fluid, and simplifying, we find

$$\mathbf{U}\cdot\mathbf{F} = -Q^{PDF}\Delta P^{T} - \iint_{P} \mathbf{u}^{PDF}\cdot\mathbf{f}^{T}\,\mathrm{d}S, \tag{3.3}$$

where the superscript T denotes that the underlying value corresponds to particle translation. Repeating for a particle rotating with angular velocity $\mathbf{W}$ in an otherwise quiescent fluid, we find that the torque exerted on a particle that is held stationary in pressure-driven flow, $\mathbf{T}$, is given by

$$\mathbf{W}\cdot\mathbf{T} = -Q^{PDF}\Delta P^{R} - \iint_{P} \mathbf{u}^{PDF}\cdot\mathbf{f}^{R}\,\mathrm{d}S, \tag{3.4}$$

where the superscript R signifies that the underlying value corresponds to particle rotation. The last two equations provide us with the components of the force and torque in the directions of the translational and angular velocities, in terms of the corresponding pressure changes and particle tractions. Unfortunately, it does not appear possible to derive a corresponding expression for the particle-induced pressure change in pressure-driven flow in terms of known results for translation and rotation.

3.2. Particle moving under a specified force and torque

In practical applications, the force, $\mathbf{F}$, and torque, $\mathbf{T}$ exerted on the particle are specified, and the particle translational and angular velocities are computed as part of the solution. This mobility problem can be formulated by extending the linear system (2.19) corresponding to the resistance problem to

$$\left[\begin{array}{c|c|c||c|c} \mathbf{P}_P & \mathbf{e}_V & \mathbf{e}_\Omega & \mathbf{P}_C & \mathbf{p}_T \\ \hline \mathbf{q}_P & 0 & \mathbf{0} & \mathbf{0} & \mathbf{0} \\ \hline \mathbf{h}_P & 0 & \mathbf{0} & \mathbf{0} & \mathbf{0} \\ \hline \mathbf{C}_P & \mathbf{0} & \mathbf{0} & \mathbf{C}_C & \mathbf{c}_T \\ \hline \mathbf{w}_P & \mathbf{0} & \mathbf{0} & \mathbf{0} & 1 \end{array}\right] \cdot \left[\begin{array}{c} \mathbf{f}_P \\ \mathbf{V} \\ \boldsymbol{\Omega} \\ \mathbf{f}_C \\ p_T \end{array}\right] = \left[\begin{array}{c} \mathbf{b}_P \\ \mathbf{F} \\ \mathbf{T} \\ \mathbf{0} \\ 0 \end{array}\right], \tag{3.5}$$

where $\mathbf{q}_P$, $\mathbf{h}_P$ are appropriate $3\times 3N_P$ sub-matrices compiled such that the second and third blocks of (3.5) are the discrete manifestations of the scalar components of (2.5), and $\mathbf{e}_V$, $\mathbf{e}_\Omega$ are appropriate $3N_P\times 3$ sub-matrices accommodating the boundary condition of rigid-body motion at the particle collocation points. The solution can be found by a variant of the iterative method discussed in Section 2.1, where the iterations are based on the block diagonalization indicated by the double horizontal and vertical partitioning lines on the left-hand side of (3.5).

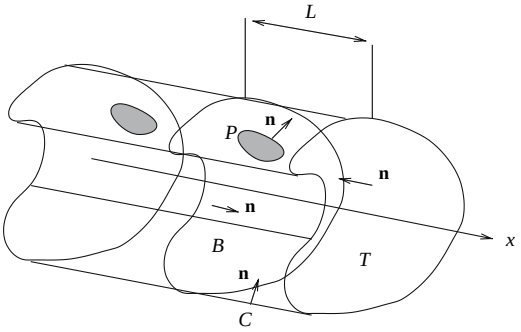

Figure 2. Schematic illustration of periodic flow through a cylindrical tube with arbitrary cross-section.

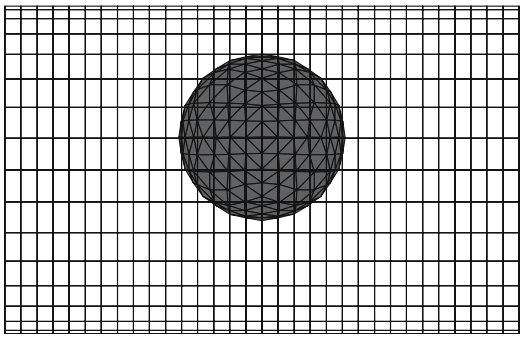

Figure 3. Discretization of the surface of a spherical particle into $N_P = 512$, six-node curved elements, and of the surface of the cylinder into $N_C = 32 \times 32 = 1024$ quadrilateral elements with two straight and two circular edges. In the boundary-element method, the traction components are approximated with constant functions over each element.

3.3. Periodic flow in a tube

The expressions for the pressure difference due to the motion or presence of an effectively isolated particle can be generalized to periodic flow through a straight or circular tube with arbitrary cross-section, as illustrated in Figure 2. In the case of a straight tube, the periodicity condition requires that the velocity distributions over two planar or warped cross-sections of the tube that are periodic images of one another in the downstream direction, x, denoted as B ant T in Figure 2, are identical.

Working as in Section 2.1, we derive the integral identity (2.7) involving the flow of interest due to the motion of the periodic array of particles, and the pure-fluid pressure-driven flow. Next, we note that the velocity of both flows is zero over the conduit surface, and simplify by the use of the aforementioned periodicity condition for the velocity to find

$$\iint_P \mathbf{u}\cdot\mathbf{f}^{PDF}\,\mathrm{d}S + \Delta p^{PDF} Q = \iint_P \mathbf{u}^{PDF}\cdot\mathbf{f}\,\mathrm{d}S + \Delta p Q^{PDF}, \tag{3.6}$$

where

$$Q \equiv \iint_B \mathbf{u}\cdot\mathbf{n}\,\mathrm{d}S = -\iint_T \mathbf{u}\cdot\mathbf{n}\,\mathrm{d}S \tag{3.7}$$

is the streamwise flow rate of the flow due to the particles. Working as in Section 2.1, we find

$$\Delta p = \frac{1}{Q^{PDF}}\left(Q\Delta p^{PDF} - \iint_P \mathbf{u}^{PDF}\cdot\mathbf{f}\,\mathrm{d}S\right). \tag{3.8}$$

We may now specify either Q or Δp, and solve for the complementary unknown using the boundary-element method described earlier in Section 2.

3.4. Multi-particle arrangements and suspensions

All of the preceding results can be generalized to multi-particle arrangements and suspension flows, by replacing the particle surface, P, with the union of the particle surfaces. The results for the pressure change in periodic flow in a cylindrical tube are especially noteworthy because of their applicability in dynamical simulations of the flow of suspensions where periodic boundary conditions are imposed.

4. Particle motion in a circular cylinder

In the case of a cylindrical tube with a circular cross-section of radius b, depicted in Figure 1(b), we use the parabolic profile of the unidirectional Poiseuille flow, $u_x^{PDF}(\sigma) = V_c(1-\sigma^2/b^2)$, and Poiseuille's law, $Q^{PDF} = \frac{1}{2}V_c\pi b^2$, where V_c is the centerline velocity, and σ is the distance from the tube axis. Expression (2.11) for the pressure difference then takes the specific form

$$\Delta p = -\frac{2}{\pi b^2}\iint_P \left(1-\frac{\sigma^2}{b^2}\right) f_x \,\mathrm{d}S. \tag{4.1}$$

Setting $p_B = 0$ and approximating the integral with a sum of integrals over the particle surface elements, we obtain

$$p_T = -\frac{2}{\pi b^2}\sum_{i=1}^{N_P}\left(1-\frac{\sigma_i^2}{b^2}\right) S_i f_{x_i}, \tag{4.2}$$

where the subscript i denotes evaluation at the centroid of the ith element, and S_i is the element surface area. Comparing this expression with (2.20), we deduce the ith component of the dimensionless vector $\mathbf{w}_P$,

$$w_{P_i} = \frac{2}{\pi b^2}\left(1-\frac{\sigma_i^2}{b^2}\right) S_i, \tag{4.3}$$

for $i = 1, \ldots, N_P$, and $w_{P_i} = 0$ for $i = N_P+1, \ldots, 3N_P$.

Since the normal vector points against the x axis over the top cap, the components of the top-cap integral vectors $\mathbf{p}_T$ and $\mathbf{c}_T$ shown in (2.19) contain the x, y, and z components of the diskoidal integral

$$\iint_T G_{xi}(\mathbf{x}, \mathbf{x}_0)\mathrm{d}S(\mathbf{x}), \tag{4.4}$$

evaluated at the particle or cylinder collocation points, $\mathbf{x}_0$. In the numerical method, these integrals were computed by applying the trapezoidal rule with 128 divisions to integrate with respect to the azimuthal angle, φ, and the 20-point Gaussian quadrature to integrate with respect to the radial position, σ.

4.1. Boundary-element method

The boundary-element method outlined in Section 2.3 was implemented for a particle with arbitrary shape and size. The particle surface was discretized into N_P quadratic elements defined by 6 nodes, descending from the successive subdivision of a regular octahedron (*e.g.*, [24]). Figure 3 shows the discretization of the surface of a spherical particle for $N_P = 512$ used for the computations discussed later in this section. The surface of a truncated section of the cylinder of length L was divided into cylindrical quadrilateral elements whose edges are defined by the intersections of N_x evenly spaced planes that are normal to the x axis, and N_φ evenly spaced azimuthal planes, as shown in Figure 3. The total number of boundary elements over the cylindrical surface is $N_C = N_x \times N_\varphi$.

The influence coefficients consisting of integrals of the Green's function over the particle elements were computed by standard boundary-element methods [24]. The corresponding influence coefficients over the cylindrical elements were computed either by a double quadrature, or by first performing the integration analytically with respect to x, and then applying

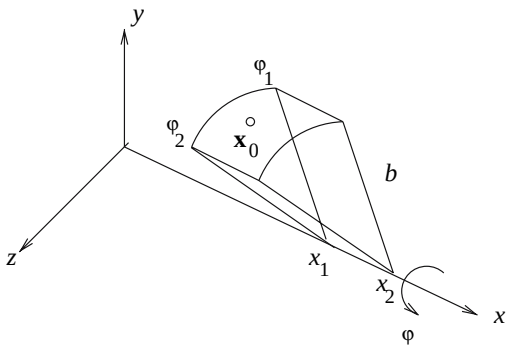

Figure 4. The single-layer influence coefficients over a cylindrical element are computed by performing the x-integration analytically, and the ϕ integration numerically.

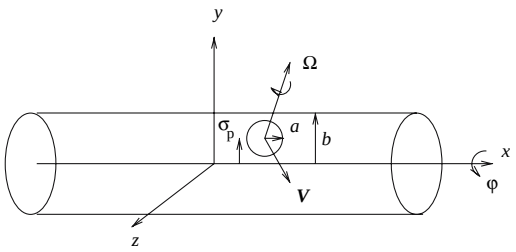

Figure 5. Illustration of a spherical particle of radius a, translating and rotating inside a circular tube of radius b.

the 6-point Gauss-Legendre quadrature to integrate with respect to φ. The second method is necessary for handling the logarithmic singularity of the integrand over singular elements. To perform the analytical integration, we consider a cylindrical element of radius b, as depicted in Figure 4, and express the influence coefficient in the form

$$\begin{aligned} I_{ij}(\mathbf{x}_0) &\equiv \iint_E G_{ij}(\mathbf{x}, \mathbf{x}_0)\, \mathrm{d}S(\mathbf{x}) \\ &= b \int_{\varphi_1}^{\varphi_2} \int_{x_1}^{x_2} \left(\frac{\delta_{ij}}{|\mathbf{x}-\mathbf{x}_0|} + \frac{(x_i - x_{0_i})\,(x_j - x_{0_j})}{|\mathbf{x}-\mathbf{x}_0|^3} \right) \mathrm{d}x\, \mathrm{d}\varphi, \end{aligned} \tag{4.5}$$

where E denotes the element. Substituting for the integration point $y = b\cos\varphi$, $z = b\sin\varphi$, and for the evaluation point $y_0 = \sigma_0 \cos\varphi_0$, $\sigma_0 = a\sin\varphi_0$, where σ_0 is the distance of the evaluation point $\mathbf{x}_0$ from the x axis, and writing

$$|\mathbf{x}-\mathbf{x}_0|^2 = (x-x_0)^2 + (b+\sigma_0)^2 - 4b\sigma_0 \cos\frac{\hat{\phi}}{2}, \tag{4.6}$$

where $\hat{\varphi} = \phi - \phi_0$, we find

$$I_{ij}(\mathbf{x}_0) = b \int_{\varphi_1}^{\varphi_2} K_{ij}(x_1, x_2, \varphi, x_0, \varphi_0)\, \mathrm{d}\varphi. \tag{4.7}$$

The φ-dependent kernels are given by

$$\begin{aligned} K_{xx} &= 2\mathcal{F} - \frac{x_2 - x_0}{|\mathbf{x}_2 - \mathbf{x}_0|} + \frac{x_1 - x_0}{|\mathbf{x}_1 - \mathbf{x}_0|}, \\ K_{xy} &= -(b\cos\varphi - \sigma_0\cos\varphi_0) \left(\frac{1}{|\mathbf{x}_2 - \mathbf{x}_0|} - \frac{1}{|\mathbf{x}_1 - \mathbf{x}_0|} \right), \\ K_{xz} &= -(b\sin\varphi - \sigma_0\sin\varphi_0) \left(\frac{1}{|\mathbf{x}_2 - \mathbf{x}_0|} - \frac{1}{|\mathbf{x}_1 - \mathbf{x}_0|} \right), \\ K_{yy} &= \mathcal{F} + \frac{(b\cos\varphi - \sigma_0\cos\varphi_0)^2}{(b+\sigma_0)^2 - 4b\sigma_0\cos\frac{\hat{\phi}}{2}} \left(\frac{x_2 - x_0}{|\mathbf{x}_2 - \mathbf{x}_0|} - \frac{x_1 - x_0}{|\mathbf{x}_1 - \mathbf{x}_0|} \right), \\ K_{yz} &= \frac{(b\cos\varphi - \sigma_0\cos\varphi_0)(b\sin\varphi - \sigma_0\sin\varphi_0)}{(b+\sigma_0)^2 - 4b\sigma_0\cos\frac{\hat{\phi}}{2}} \left(\frac{x_2 - x_0}{|\mathbf{x}_2 - \mathbf{x}_0|} - \frac{x_1 - x_0}{|\mathbf{x}_1 - \mathbf{x}_0|} \right), \\ K_{zz} &= \mathcal{F} + \frac{(b\sin\varphi - \sigma_0\sin\varphi_0)^2}{(b+\sigma_0)^2 - 4b\sigma_0\cos\frac{\hat{\phi}}{2}} \left(\frac{x_2 - x_0}{|\mathbf{x}_2 - \mathbf{x}_0|} - \frac{x_1 - x_0}{|\mathbf{x}_1 - \mathbf{x}_0|} \right), \end{aligned} \tag{4.8}$$

where

$$\mathcal{F} \equiv \log\Big(\frac{x_2 - x_0 + |\mathbf{x}_2 - \mathbf{x}_0|}{x_1 - x_0 + |\mathbf{x}_1 - \mathbf{x}_0|}\Big). \tag{4.9}$$

When $\sigma_0 = a$ and $x_1 \le x_0 \le x_2$, whereupon the evaluation point lies in the tube section hosting the element, a logarithmic singularity occurs in the function $\mathcal{F}$ as $\varphi \to \varphi_0$. To compute the corresponding integral, we regularize the integrand by writing

$$\mathcal{F} = \log\Big(\frac{x_2 - x_0 + |\mathbf{x}_2 - \mathbf{x}_0|}{x_1 - x_0 + |\mathbf{x}_1 - \mathbf{x}_0|}\,(\varphi - \varphi_0)^2\Big) - \log(\varphi - \varphi_0)^2, \tag{4.10}$$

and then perform the integration of the second term on the right-hand side by elementary methods.

4.2. A spherical particle translating parallel to the tube axis

As a first case study, we consider the flow induced by a translating spherical particle of radius a, positioned at a distance σ_P from the tube axis, as illustrated in Figure 5. Since translation normal to the cylinder generators does not produce a pressure difference, Δp, we confine our attention to the case of motion along the tube axis.

For sufficiently small particle to tube radius ratio, $\delta \equiv a/b$, we may apply the asymptotic expression (2.17) to obtain the estimate

$$\Delta p \simeq \frac{12\mu a V_x}{b^2}\,(1 - \beta^2), \tag{4.11}$$

accurate to first order in δ, where $\beta \equiv \sigma_P/b$ is the reduced radial particle position, and V_x is the particle velocity. Motivated by this expression, we introduce the dimensionless pressure coefficient $c_T(\beta, \delta)$, defined by

$$\Delta p \equiv \frac{12\mu a V_x}{b^2}\,(1 - \beta^2)\,c_T, \tag{4.12}$$

where $c_T(\beta, \delta \to 0) = 1$. Happel and Byrne [1] and Greenstein and Happel [4] performed a detailed calculation using the method of reflections, and derived the asymptotic expansion

$$c_T = 1 + f(\beta)\ \delta + \Big(f^2(\beta) - \frac{2}{3(1-\beta^2)}\Big)\,\delta^2 + O(\delta^3). \tag{4.13}$$

The function $f(\beta)$ monotonically decreases from $f(0) = 2{\cdot}10444$ to $f(0{\cdot}40) = 2{\cdot}04388$, and then increases to $f(0{\cdot}90) = 5{\cdot}30$ (*e.g.*, [4]).

4.2.1. *Axisymmetric flow*

Wang and Skalak [3] presented numerical results for a particle positioned at the cylinder axis, $\sigma_P = 0$ and $\beta = 0$, corresponding to axisymmetric flow. In particular, in their Table 5, these authors list a pressure coefficient, P_U, that is related to the present pressure coefficient by $c_T = \delta P_U/12$. Setting $\beta = 0$ and $f(0) = 2{\cdot}10444$, we find that Greenstein and Happel's [4] expansion for axial translation in axisymmetric flow takes the specific form

$$c_T = 1 + 2{\cdot}10444\ \delta + 3{\cdot}7620\ \delta^2 + O(\delta^3). \tag{4.14}$$

In an earlier study, Happel and Byrne [1] derived the more accurate Padé-like expansion

$$c_T = \frac{1 - \frac{2}{3}\,\delta^2}{1 - f(0)\,\delta + 2{\cdot}087\,\delta^3}. \tag{4.15}$$

To second-order in δ, (4.15) reduces to (4.14).

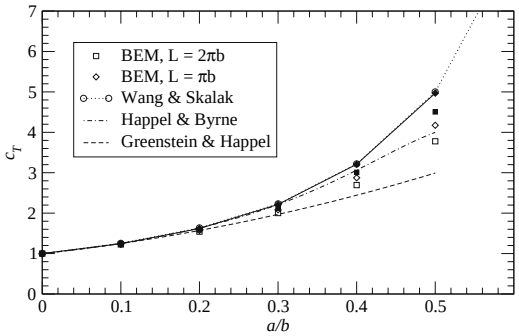

Figure 6. Graph of the pressure coefficient, c_T, plotted against the particle to cylinder radius ratio, $\delta = a/b$, for a sphere translating along the axis of a cylindrical tube.

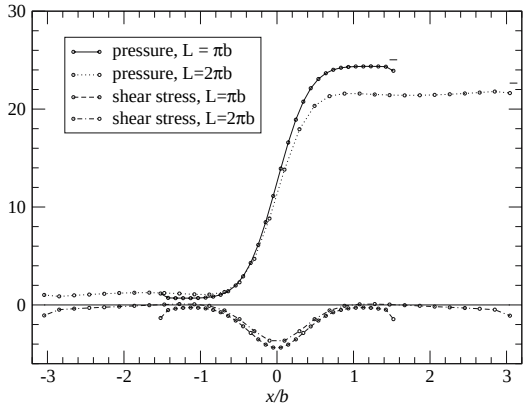

Figure 7. Distribution of the normalized pressure and shear stress along the cylinder length for a particle of radius $a = 0{\cdot}5b$, translating along the cylinder axis, for two cylinder truncation levels.

Figure 6 shows a graph of the pressure coefficient, c_T, plotted against the particle to cylinder radius, a/b, for small and moderate particle radii. The hollow squares and diamonds represent results of boundary-element computations for cylinder truncation levels, respectively, $L = 2\pi b$ and πb, $N_P = 512$ particle elements, and $N_C = 32 \times 32 = 1024$ cylinder elements. In a previous calculation, Mondy *et al.* [10] used a maximum of 176 cylinder elements. The computation of the inverses of the corresponding self-interaction matrices discussed in Section 2 requires, respectively, 20 and 250 min of CPU time on a 2·4 GHz processor. The dashed line represents the asymptotic results of Greenstein and Happel [4] expressed by (4.14), the dot-dashed line represents the asymptotic results of Happel and Byrne [1] expressed by (4.15), and the circles connected by the dotted line represent the numerical results of Wang and Skalak [3, Table 5]. The accuracy of the boundary-element computations is excellent or very good for particle radii $a < 0{\cdot}3\,b$, but the numerical error becomes substantial for higher particle radii due to the small number of boundary elements over the tube wall. The filled squares and diamonds show the results of the heuristic correlation, $\Delta P \simeq -2\ F_{P_x}/(\pi b^2)$, where F_{P_x} is the x-component of the force exerted on the particle, computed using the boundary-element method. It is interesting that the heuristic correlation is in excellent agreement with the virtually exact results of Wang and Skalak [3], even for larger particle radii.

Figure 7 illustrates the distribution of the pressure and shear stress along the cylinder length, both rendered dimensionless by $\mu V_x/b$, for a particle of radius $a = 0{\cdot}5b$. On a no-slip surface, the pressure is equal to the negative of the normal component of the traction. Results in Figure 7 are shown for cylinder truncation levels, $L = 2\pi b$ and πb, with the short horizontal segments on the right end of each distribution for the pressure representing the top cylinder-cap pressure, as it emerges from the boundary-element solution. The graphs show that the short truncation length, $L = \pi b$, is long enough for the shear stress and pressure to reach the upstream and downstream plateaus. For this particle size, the fineness of the cylinder surface discretization determined by the truncation level has a significant effect on the accuracy of the boundary-element solution.

The distribution of the shear stress for $L = \pi b$ shown in Figure 7 remains negative over the whole of the computational domain. The corresponding distribution for $L = 2\pi b$ changes sign twice, once at $x/b \simeq 1{\cdot}0$ and then at 1·6. The change in sign is consistent with the formation

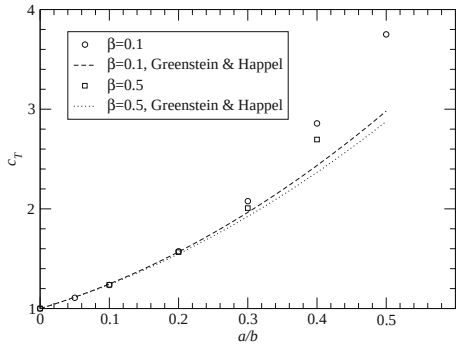

Figure 8. Graph of the pressure coefficient, c_T, for a sphere translating off the axis of a cylindrical tube.

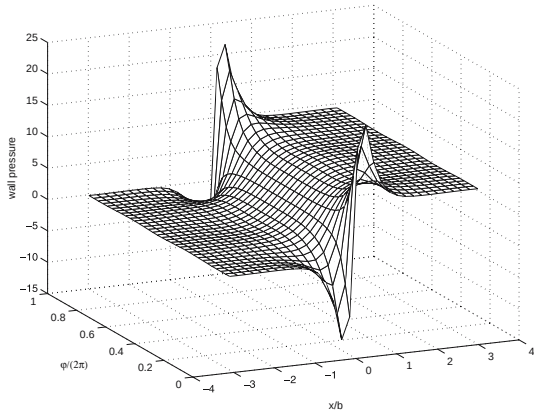

Figure 9. Distribution of the normalized pressure over the cylinder wall induced by a particle of radius $a = 0{\cdot}4b$ translating at a distance $\sigma_P = 0{\cdot}5b$ from the tube axis.

of toroidal eddies of the flow due a point force identified by Liron and Shahar [16] and Blake [17].

4.2.2. *Non-axisymmetric flow*

Next, we consider the pressure change due to a particle translating off and parallel to the cylinder axis, generating a non-axisymmetric flow. Figure 8 shows a graph of the pressure coefficient, c_T, plotted against the particle to cylinder radius ratio, a/b, for radial particle center positions $\beta \equiv \sigma_P/b = 0{\cdot}1$ and $0{\cdot}5$. The symbols represent the results of the present boundary-element computations with the aforementioned number of boundary elements and cylinder truncation level $L = \pi b$, and the broken lines represent the predictions of the Greenstein and Happel [4], expressed by (4.13). As in the case of axial translation along the centerline, the asymptotic results are surprisingly accurate even for moderate particle radii, though they tend to underestimate the pressure coefficient for larger particle sizes.

Figure 9 illustrates the distribution of the pressure rendered dimensionless by $\mu V_x/b$ over the cylinder wall, for a particle of radius $a = 0{\cdot}4b$, translating at a distance $\sigma_P = 0{\cdot}5b$ from the tube axis. The clearance of the particle surface from the wall is $0{\cdot}10b$, The 32×32 grid displayed in this graph corresponds to the actual cylinder-element tessellation employed in the computations over the truncated length $L = \pi b$. The results show that large pressure variations occur near the region of minimum particle-wall separation due to the local lubrication flow, while the transition from the upstream to the downstream pressure elsewhere is smooth. Far upstream, the cylinder pressure is nearly equal to the cap pressure plotted in Figure 8.

4.3. A spherical particle rotating transversely to the tube axis

As a second case study, we consider the flow induced by a spherical particle rotating about its center inside a cylindrical tube. Since, by symmetry, rotation around the axis that is parallel to the generators or normal to the tube axis generates neither a net force on the particle nor a pressure difference across the tube, we consider rotation around an axis that points in the azimuthal direction with angular velocity Ω_φ. Greenstein and Happel [4] derived the asymptotic prediction

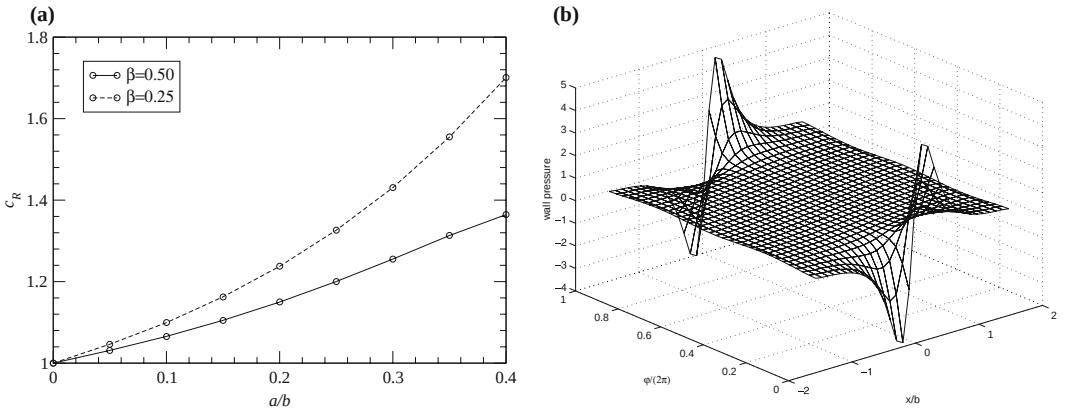

Figure 10. (a) Graph of the pressure coefficient, c_R, against the reduced particle radius, for a sphere rotating in the azimuthal direction, for reduced radial particle center position β = 0·25 and 0·50. (b) Distribution of the normalized pressure over the cylinder wall for a particle of radius $a = 0{\cdot}4\ b$ positioned at $\beta = 0{\cdot}50$.

$$\Delta p = \frac{16\mu a^3 \Omega_\varphi}{b^3} \beta \left(1 + O(\delta)\right), \tag{4.16}$$

which motivates the definition

$$\Delta P = \frac{16\mu a^3 \Omega_\varphi}{b^3} \beta\, c_R, \tag{4.17}$$

where $c_R(\delta, \beta)$ is a pressure change coefficient for rotation. When the particle is located at the tube axis, $\beta = 0$, the pressure field is fore-and-aft symmetric, and a pressure difference does not appear.

Figure 10(a) shows a graph of the pressure coefficient, c_R, for a particle situated a quarter and midway along a tube radius, $\beta = 0{\cdot}25$ and 0·5, computed by the boundary-element method with the element discretization discussion in Section 4.2, and cylinder truncation level $L = \pi b$. To the author's knowledge, the numerical results presented in this figure provide the first independent confirmation of the correctness of Greenstein and Happel's [4] asymptotic prediction for the pressure rise in rotation.

As in the case of axial translation, as the particle radius increases, the pressure coefficient rises at a nearly linear rate above the asymptotic value of unity. Thus, wall effects accentuate the pressure change. Figure 10(b) illustrates the distribution of the pressure rendered dimensionless by $\mu\Omega_\varphi$ over the cylinder wall, for a particle of radius $a = 0{\cdot}4b$, and for $\beta = 0{\cdot}50$. Compared to translation, rotation induces a smaller pressure rise relative to the pronounced peaks occurring in the gap between the particle surface and the wall.

4.4. A translating oblate spheroid

As a last case study, we consider the flow induced by the translation of an oblate spheroid with aspect ratio 2·0 and equivalent to tube radius ratio, $a/b = 0{\cdot}35$, where the equivalent radius is related to the particle volume, V, by the equation $V = 4\pi a^3/3$. The minimum and maximum particle semi-axes are, respectively, $0{\cdot}2205\,b$ and $0{\cdot}4410\,b$, to shown accuracy. The spheroid is positioned with the flat face normal to the xy plane rotated at an angle φ_z with respect to the z-axis, while the particle center lies on the tube axis, as illustrated in Figure 11. Particle translation along the x-axis generates axisymmetric flow only in the transverse configuration corresponding to $\varphi_z = 0$. For any other configuration, the flow is genuinely three-dimensional. Both configurations shown in Figure 11 have been observed in laboratory

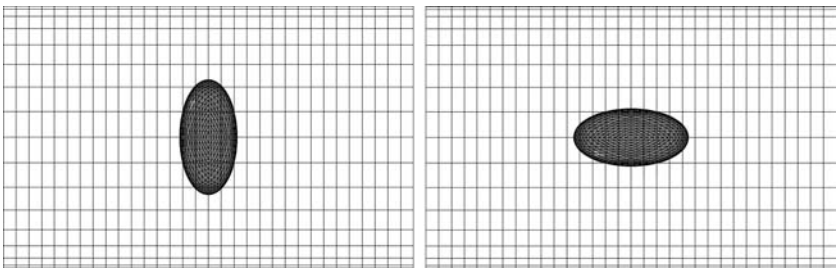

Figure 11. Discretization of an oblate spheroid with axes ratio equal to 2 and reduced equivalent ratio $a/b = 0{\cdot}35$ in the transverse (left) and lateral (right) configuration, corresponding to $\phi_z = 0$ and $\pi/2$, respectively.

studies of red blood cell motion through microcapillaries, with the transverse configuration being more common (*e.g.*, [25,26]).

The boundary-element solution yields among other results the dimensionless drag force coefficient, defined as $c_{T_D} \equiv -F_x/(6\pi\mu a V_x)$, where F_x is the force acting on the particle in axial translation with velocity V_x. For particle surface discretization into $N_P = 512$ elements, and $N_C = 1024$ cylindrical elements over the truncated length $L = \pi b$, as shown in Figure 11, the computed drag coefficient, c_{T_D}, is 3·76, 3·13, and 2·55, and the computed pressure difference coefficient, c_T, is 3·29, 2·81, and 2·35, respectively, for orientation angles $\varphi_z = 0$, $\pi/4$, and $\pi/2$. Thus, both coefficients decrease as the spheroid is rotated from the transverse to the lateral configuration, which is believed to be a new result. For reference, we note that the computed drag coefficient for a spherical particle of radius a is $c_{T_D} = 2{\cdot}65$, and the corresponding pressure difference coefficient is $c_T = 2{\cdot}43$, which are somewhat higher than the corresponding coefficients for the lateral configuration. Based on the comparison between the numerical results with the exact solution presented in Figure 6, the boundary-element numerical solution is expected to carry an error on the order of 5% for this particle size. Indeed, a theoretical calculation using Bohlin's method of reflections (*e.g.*, [27, p. 318] shows that, for a spherical particle of radius $a/b = 0{\cdot}35$, the drag coefficient is $c_{T_D} = 2{\cdot}81$.

5. Discussion

We have shown that expressing the pressure rise induced by a suspended particle in tube flow as an integral of the *a priori* unknown particle traction facilitates and simplifies the numerical implementation of the boundary-element method. It is possible that the integral representation for the pressure difference can be used in lieu of a downstream boundary condition in Stokes flow computations using domain discretization method, including the finite-volume and finite-element method, though testing this proposition is a topic for further research. Some of the results of the numerical computations presented in this article using an entry-level boundary-element method duplicate and confirm those of previous authors, while others add to the data bank of particulate Stokes-flow hydrodynamics.

The theoretical results and algorithms developed in this article for rigid particles can be extended in a straightforward fashion to bubbles, drops, and capsules enclosed by thin membranes, in tube flow. Consider the flow induced by the motion of a liquid capsule in a fluid-filled tube that is closed at both ends. Assuming that the velocity is continuous across the interface, and applying the reciprocal theorem for the exterior and interior capsule flow, we find that the induced pressure rise is given by [25,26]

$$\Delta P = -\frac{1}{Q^{PDF}} \iint_D \Delta\mathbf{f} \cdot \mathbf{u}^{PDF} \, \mathrm{d}S - \frac{\lambda - 1}{Q^{PDF}} \iint_D \mathbf{f}^{PDF} \cdot \mathbf{u} \, \mathrm{d}S, \tag{5.1}$$

where D stands for the capsule surface, λ is the ratio of the capsule fluid to the ambient fluid viscosity, and $\Delta\mathbf{f}$ is the jump in the interfacial traction due to an interfacial tension field. The integral representation (5.1) is the counterpart (2.11) for interfacial flow. In the implementation of the boundary-element method, the integral representation (5.1) can be used to relate the pressure difference across the tube to the jump in the interfacial traction and interfacial velocity. The latter is given by an integral representation in the case of equal viscosities, $\lambda = 1$, or must be computed by solving an integral equation of the second kind in the case of unequal viscosities.

The basic boundary-element implementation presented in this article can be improved by employing high-order and spectral-element expansions (*e.g.*, [11]). Furthermore, multi-particle arrangements and periodic flows can be addressed by straightforward extensions. Of particular interest due to its relevance in biomechanics is the motion of particles in bifurcating tubes. The development of the pertinent algorithms is currently under way.

Acknowledgement

This research was supported by a grant provided by the National Science Foundation.

References

1. J. Happel and B.J. Byrne, Motion of a sphere and fluid in a cylindrical tube. *Ind. Eng. Chem.* 46 (1954) 1181–1186; corrigendum in *Ind. Eng. Chem.* 49 (1957) 1029.
2. W.L. Haberman and R.M. Sayre, Motion of rigid and fluid spheres in stationary and moving liquid inside cylindrical tubes. David Taylor Basin Report 1143, Washington, DC (1969).
3. H. Wang and R. Skalak, Viscous flow in a cylindrical tube containing a line of spherical particles. *J. Fluid Mech.* 38 (1969) 75–96.
4. T. Greenstein and J. Happel, Theoretical study of the slow motion of a sphere and a fluid in a cylindrical tube. *J. Fluid Mech.* 34 (1968) 705–710.
5. H. Tözeren, Torque on eccentric spheres flowing in tubes. *J. Appl. Mech.* 49 (1982) 279–283.
6. H. Tözeren, Drag on eccentric spheres translating and rotating in tubes. *J. Fluid Mech.* 129 (1983) 77–90.
7. H. Tözeren, Application of boundary integral equation method to some Stokes problems. *J. Num. Meth. Fluids* 4 (1984) 159–170.
8. A.L. Graham, L.A. Mondy, J.D. Miller, N.J. Wagner and W.A. Cook, Numerical simulations of eccentricity and end effects in falling ball rheometry. *J. Rheol.* 33 (1989) 1107–1128.
9. M.S. Ingber, Dynamic simulation of the hydrodynamic interaction among immersed particles in Stokes flow. *Int. J. Num. Meth. Fluids* 10 (1990) 791–809.
10. L.A. Mondy, M.S. Ingber and S.E. Dingman, Boundary element method simulations of a ball falling through quiescent suspensions. *J. Rheol.* 35 (1991) 825–848.
11. J.J.L. Higdon and G.P. Muldowney, Resistance functions for spherical particles, droplets and bubbles in cylindrical tubes. *J. Fluid Mech.* 298 (1995) 193–210.
12. G.-H. Zheng, R.L. Powell and P. Stroeve, Torque and frictional force acting on a slowly rotating sphere arbitrarily positioned in a circular cylinder. *Ind. Eng. Chem. Res.* 31 (1992) 1190–1194.
13. T.C. Chen and R. Skalak, Stokes flow in a cylindrical tube containing a line of spheroidal particles. *Appl. Sci. Res.* 22 (1970) 403–441.
14. A. Falade and H. Brenner, First-order wall curvature effects upon the Stokes resistance of a spherical particle moving in close proximity to a solid wall. *J. Fluid Mech.* 193 (1988) 533–568.
15. C. Pozrikidis, *Boundary Integral and Singularity Methods for Linearized Viscous Flow.* Cambridge: Cambridge University Press (1992) 259 pp.
16. N. Liron and R. Shahar, Stokes flow due to a Stokeslet in a pipe. *J. Fluid Mech.* 86 (1978) 727–744.
17. J.R. Blake, On the generation of viscous toroidal eddies in a cylinder. *J. Fluid Mech.* 95 (1979) 209–222.
18. B.R. Hirschfeld, *A Theoretical Study of the slow asymmetric settling of an arbitrarily-positioned particle in a circular cylinder.* Ph.D. Dissertation. New York: New York University (1972).

19. H. Hasimoto, Slow motion of a small sphere in a cylindrical domain. *J. Phys. Soc.* 41 (1976) 2143–2144; 42 (1976) 1047.
20. B.R. Hirschfeld, H. Brenner and A. Falade, First- and second-order wall effects upon the slow viscous asymmetric motion of an arbitrarily-shaped, -positioned, and -oriented particle within a circular cylinder. *Physicochem. Hydrodyn.* 5 (1984) 99–133.
21. C. Couillette and C. Pozrikidis, Motion of liquid drops through tubes. *J. Fluid Mech.* 358 (1998) 1–28.
22. H.K. Kuiken, H.A. Lorentz, sketches of his work on slow viscous flow and some other areas in fluid mechanics and the background against which it arose. *J. Engng. Math.* 30 (1996) 1–18.
23. H. Brenner, Pressure drop due to the motion of neutrally buoyant particles in duct flows. *J. Fluid Mech.* 43 (1970) 641–660.
24. C. Pozrikidis, *A Practical Guide to Boundary-Element Methods with the Software Library BEMLIB.* Boca Raton: Chapman & Hall/CRC (2002) 423 pp.
25. C. Pozrikidis, Axisymmetric motion of a file of red blood cells through capillaries. *Phys. Fluids* (in press).
26. C. Pozrikidis, Numerical simulation of cell motion in tube flow. *Annals Biomed. Engng.* (in press).
27. J. Happel and H. Brenner, *Low Reynolds number hydrodynamics.* Dordrecht: Martinus Nijhoff (1986) 553 pp.